

Structural rotation of Al under uniaxial compression: A first-principles prediction

S. K. Yadav,^{1,2} J. Wang,¹ R. Ramprasad,² A. Misra,³ and X.-Y. Liu^{1,a)}¹Materials Science and Technology Division, MST-8, Los Alamos National Laboratory, Los Alamos, New Mexico 87545, USA²Chemical, Materials and Biomolecular Engineering, Institute of Materials Science, University of Connecticut, Storrs, Connecticut 06269, USA³Materials Physics and Applications Division, MPA-CINT, Los Alamos National Laboratory, Los Alamos, New Mexico 87545, USA

(Received 25 April 2012; accepted 20 July 2012; published online 29 August 2012)

We report on a density functional theory based study of a novel structural rotation of single-crystal aluminum (Al) under uniaxial compression. It was found that under strains either along the $\langle 112 \rangle$ or the $\langle 111 \rangle$ direction, beyond a critical stress of about 13 GPa, the Al crystal can rotate through shear in the Shockley partial direction on the $\{111\}$ plane, to relieve internal stresses. This phenomenon reveals a new mechanism leading to the onset of homogeneous dislocation nucleation in face-centered-cubic materials under high uniaxial compressions. © 2012 American Institute of Physics. [<http://dx.doi.org/10.1063/1.4747923>]

I. INTRODUCTION

Aluminum (Al) is often considered as a prototype material for understanding the high-pressure behavior of simple face-centered-cubic (fcc) metals.¹ Indeed, recent work on the phase stability of Al under high pressures has received much interest and it was predicted, using density functional theory (DFT) based simulations, that a fcc to hexagonal-close-packed (hcp) phase transformation happens under hydrostatic compression.^{2–5} In this paper, we report a DFT study in Al in which a novel structural rotation under compressive strain is identified involving collective shuffling motions. The estimated critical stress required for such crystal rotation transformations is 13 GPa for uniaxial compression along $[11\bar{2}]$ or $[111]$ direction. Incidentally, the rotational deformation mode in the plastic deformation of nanocrystals is accompanied by crystal lattice rotations, which has also attracted significant attention recently.^{5–8} Such deformation modes have been used to explain the unusual strength and plasticity behaviors of nanocrystalline solids.^{5–8} However, the detailed mechanism has not been identified.

Fig. 1 schematically shows the essence of the present findings. As Al is uniaxially compressed along the $[11\bar{2}]$ or the $[111]$ direction, it expands, respectively, in the $[1\bar{1}0]$ and $[111]$ directions, or in the $[11\bar{2}]$ and $[1\bar{1}0]$ directions. While a non-linear elastic behavior is observed before a critical stress, a spontaneous switching of the $[11\bar{2}]$, $[1\bar{1}0]$, and $[111]$ crystallographic directions to $[100]$, $[010]$, and $[001]$, respectively, occurs at a critical stress (as schematically shown in Fig. 1). This crystallographic rotation is due to coherent shuffling of atoms, and must be differentiated from simple or pure shearing, which does not involve a change of crystallographic directions.

II. METHODS

DFT simulations were carried out using the Vienna *ab initio* simulation package (VASP),⁹ with the Perdew-Burke-Ernzerhof (PBE) generalized gradient approximation (GGA) functional,¹⁰ and projector-augmented wave (PAW) frozen-core potentials.¹¹ An energy cut-off of 300 eV for the planewave expansion of the wave functions was used. The calculated and experimental values of lattice parameters, bulk modulus, and elastic constants of Al compare well,^{12,13} indicating the robustness of the computational settings chosen. To achieve a very high level of accuracy, a Monkhorst-Pack k-point mesh of $18 \times 18 \times 18$ was used in the simulations. During the simulations, the Hellmann-Feynman force of each atom in the computational supercell was converged to 0.01 eV/Å or less.

We start with a cuboid shaped supercell, with the x-, y-, and z- axes of the initial fcc crystal oriented, respectively, along the $[1\bar{1}0]$, $[11\bar{2}]$, and $[111]$ directions. Uniaxial stress loading is achieved through two steps: first, we applied a uniaxial uniform strain along the $[11\bar{2}]$ direction (y-axis of Fig. 2) and then, in the second step, we allowed stress relaxation to occur in the other two normal directions without symmetry constraints. During the relaxation, shear strains can be induced in association with the energy minimization.

III. RESULTS AND DISCUSSION

When the crystal is subjected to an uniaxial compressive stress along the y-direction (initially along $[11\bar{2}]$), Figs. 2(a)–2(e) show the structural rotation and the corresponding mechanics. The atomic structure of Al at four different strains is shown in Fig. 2(a). Configuration 1 is at equilibrium with zero strain, configuration 2 corresponds to the strained structure at strain $\varepsilon_{yy} = -0.15$ while maintaining the initial crystal orientation. Further straining to $\varepsilon_{yy} = -0.17$ leads to configuration 3, where a rotated crystal structure is observed accompanied by a shear strain of $\varepsilon_{yz} = -0.33$. This rotated structure

^{a)}Author to whom correspondence should be addressed. Email: xyliu@lanl.gov.

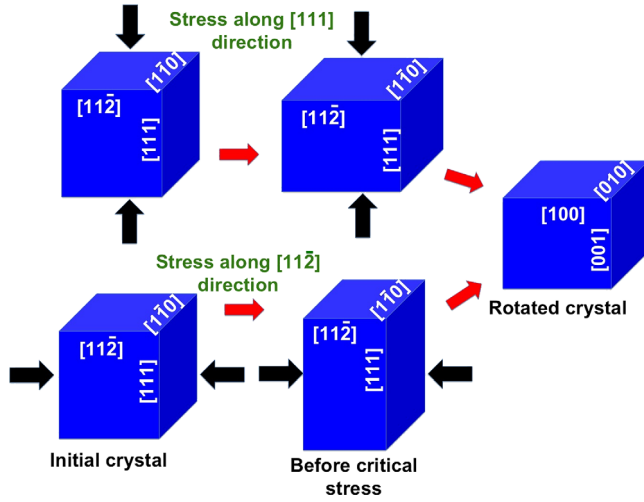


FIG. 1. Schematic of crystal rotation due to uniaxial compression along $[111]$ and $[112]$ directions. Black arrows show direction of compression.

remains at configuration 4 when the compressive strain is -0.19 . Symmetry analyses performed for configurations 3 and 4 show that they retain their fcc structure but with an orientation (now, $[100]$ //x-axis, $[010]$ //y-axis, and $[001]$ //z-axis) rotated with respect to the original fcc crystal.

Figure 2(b) shows the variation of the total energy as a function of the compressive strain. The loading before the structural rotation is accompanied by an energy increase of 0.09 eV/atom, corresponding to the activation energy barrier for this process. The compressive stress along the y-direction increases nonlinearly during the course of this process (Fig. 2(c)). The inelastic effect is also shown in Fig. 2(d) in association with the inelastic Poisson's ratios. When the compressive strain is less than -0.05 , ϵ_{xx} and ϵ_{zz} are almost equal,

but for larger strains, ϵ_{xx} increases and ϵ_{zz} decreases as ϵ_{yy} increases. When the compressive stress reaches 13.0 GPa, this inelastic deformation continues and leads to a structural instability, as evidenced by the discontinuity points in Figs. 2(b)–2(d). The structural instability induced the collective shuffling, which occurs along the $[11\bar{2}]$ direction with respect to the initial crystal. This shuffling is associated with the nucleation and glide of Shockley dislocation dipole in fcc, with Burgers vector of $\langle 11\bar{2} \rangle/6$. As a consequence, the relaxation of internal stresses (inelastic energy) drives the structural rotation from the initial fcc directions ($[1\bar{1}0]$, $[11\bar{2}]$, and $[111]$) to the new orientations ($[100]$, $[010]$, and $[001]$).

In order to clarify whether the collective shuffle assisted by in-plane shear favors structural rotation, we subjected the configurations before the structural rotation to in-plane shear stresses along $[11\bar{2}]$ (111) shear. The results provide two insights. First, the theoretical shear strength along $[11\bar{2}]$ (111) shear decreases with an increase of compressive stress (see Fig. 2(e)), which is understandable because of the increasing interplanar spacing of (111) planes. Second, shear strain does not favor structural rotation, the structural rotation occurs only when stress is high enough to break in-plane bonds along $[1\bar{1}0]$ direction. The critical bond length is found to be 0.32 nm.

Next, we carried out a second set of calculations involving compression along the $[111]$ direction to prove whether the critical bond length is a generic condition. Our results are summarized in Fig. 3. Similar to Fig. 2, Fig. 3(a) shows the crystal structure configurations of Al at four different strains, (1) 0.0 , (2) -0.18 , (3) -0.22 , and (4) -0.14 . It is noted that (1) the activation energy is higher, 0.19 eV/atom compared to 0.09 eV/atom found earlier for compression along the $[11\bar{2}]$ direction; (2) the critical stress remains similar, 13 GPa; (3) the theoretical shear strength of the (111) plane

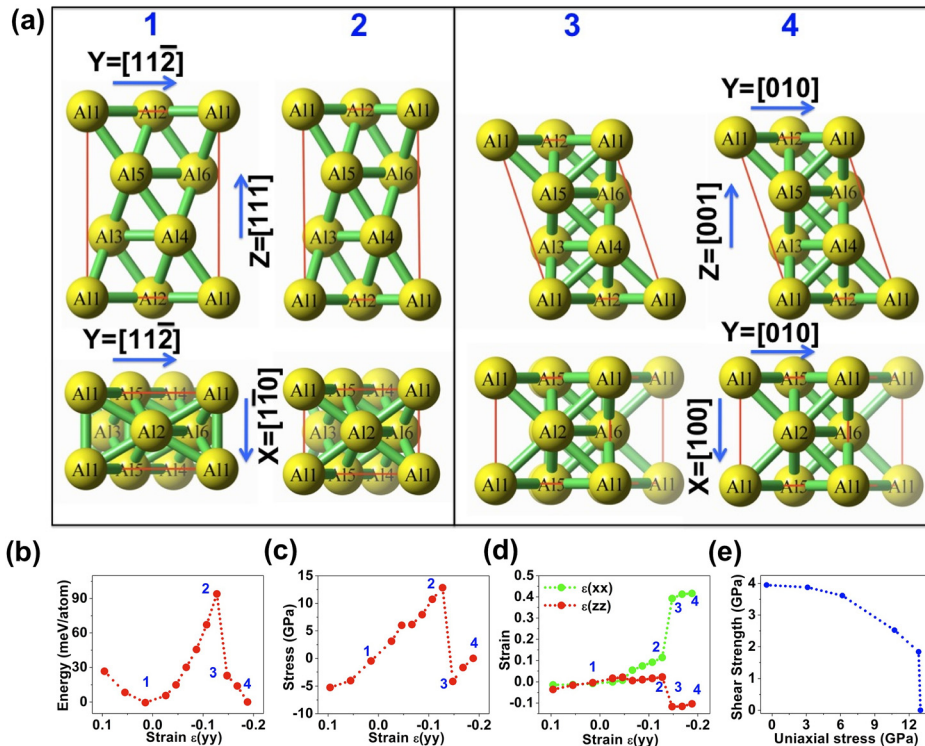


FIG. 2. (a) Atomic structures of Al crystal with respect to the compressive strains of (1) 0.0 , (2) -0.15 , (3) -0.17 , and (4) -0.19 along the y-direction ($[11\bar{2}]$). The top row is the projection along the x-direction and the lower row is the projection along the z-direction. (b) Variation of the total energy as a function of the compressive strain ϵ_{yy} . (c) The normal stress σ_{yy} as a function of the compressive strain ϵ_{yy} . (d) Variation of strains ϵ_{xx} and ϵ_{zz} as a function of strain (ϵ_{yy}) corresponding to uniaxial stress loading. (e) Shear strength of (111) along $[11\bar{2}]$ as a function of uniaxial compressive stress σ_{yy} .

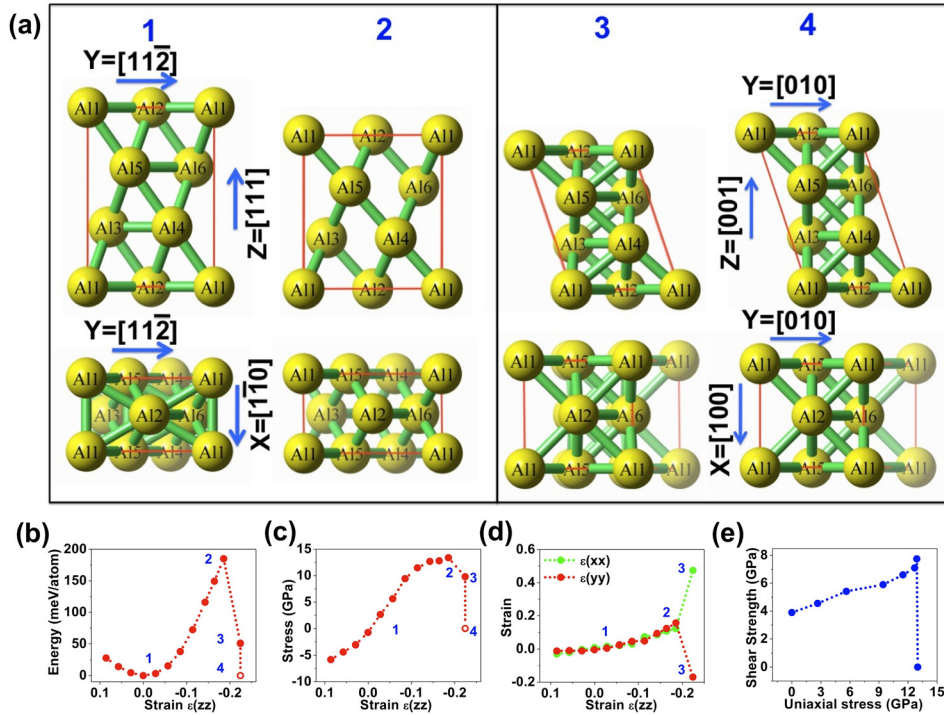


FIG. 3. (a) Atomic structures of Al crystal with respect to the compressive strains of (1) 0.0, (2) -0.18 , (3) -0.22 , and (4) -0.14 along the z-direction ([111]). The top row is the projection along the x-direction and the lower row is the projection along the z-direction. (b) Variation of the bonding energy as a function of the compressive strain ϵ_{zz} . (c) The normal stress σ_{zz} as a function of the compressive strain ϵ_{zz} . Open circles denote relaxation to final fcc crystal, this involves expansion along z direction. (d) Variation of strains ϵ_{xx} and ϵ_{yy} as a function of strain (ϵ_{zz}) corresponding to uniaxial stress loading. (e) Shear strength of (111) along [112] as a function of uniaxial compressive stress σ_{zz} .

increases with the increase of the compressive stress; (4) the structural rotation requires the collective shuffle along [112] direction; (5) the nonlinear Poisson's ratio ν_{31} and ν_{32} are identical regardless of the compressive strain ϵ_{zz} before the structural transformation; and (6) most importantly, regardless of all these differences, the critical bond length, 0.32 nm, remains equal to that in the 1st case.

Based on our DFT results for the two types of imposed strains, we can conclude that the structural rotation is achieved through the bond breaking in $[1\bar{1}0]$ direction, accompanied by “zero” shear strength on the (111) plane. The large elastic energy release during the structural transition, from a highly reduced bonding co-ordination (6 nearest neighbor bonds) to the fcc bonding co-ordination (12 nearest neighbor bonds) is the critical factor that contributes to this novel rotation phenomena. This suggests that even under a large strain, the material prefers a high co-ordination bonding environment, which is thermodynamically more stable and kinetically achievable.

In forming the rotated fcc phase under the stress conditions, the Al crystal shears in the Shockley partial direction (i.e., $[11\bar{2}]$) on (111) plane. This also indicates that in such axial compressive stress condition, the bonding situation would allow the easy shear of the Shockley partial displacement, thereby creating the opportunity to homogeneously nucleate dislocations with Shockley partial Burgers vectors, at the critical stress level of about 13 GPa. This phenomenon reveals a new mechanism leading to the onset of homogeneous dislocation nucleation in fcc materials under high uniaxial compressions. This finding, in our knowledge, has not been reported or discussed before in the literature.

Recent molecular dynamics (MD) simulations using the embedded atom method (EAM) interatomic potentials that studied uniaxial compressive stress loading on Al along the $[111]$ direction¹⁴ observed that dislocations start to form at

around 17 GPa. Although in comparison with DFT techniques, it is known that the EAM potential is less accurate in modeling high pressure or very large strain environments, the MD results in these studies validate the new dislocation nucleation mechanism under high uniaxial compressions, as discovered from the current DFT simulations.

In contrast to the semi-empirical MD results reported in Ref. 14, no local hcp environments are observed in DFT calculations. This is due to the small size of computational unit cell used in DFT calculations compared to that in MD.

IV. CONCLUSIONS

In summary, we have performed first-principles DFT based simulations to investigate the deformation of an Al crystal under uniaxial compressive strains. A novel structural transformation, i.e., coherent shuffling crystal rotation, was identified. It was found that under compressive strains along either the $[11\bar{2}]$ or $[111]$ directions, at a critical stress of about 13 GPa, the Al crystal shears in the Shockley partial direction on the (111) plane, forming a rotated fcc phase, thereby relieving the stress in the system. These results identified the critical condition for structural rotation, the bond breaking on the $\{111\}$ planes. Such condition is related to the theoretical limit of uniaxial strain in single crystal Al. Under such compressive stress conditions, the bonding situation allows the easy shear of the Shockley partial displacement. This phenomenon reveals a new mechanism leading to the onset of homogeneous dislocation nucleation in fcc materials under high uniaxial compressions.

ACKNOWLEDGMENTS

This work was supported by the US Department of Energy, Office of Science, Office of Basic Energy Sciences.

S.K.Y. and J.W. also acknowledge the support provided by the Los Alamos National Laboratory Directed Research and Development Project ER20110573. The authors acknowledge insightful discussions with Richard G. Hoagland and John P. Hirth. S.K.Y. also acknowledges helpful discussions with Anand K. Kanjarla, Enrique Martinez, and Ghanshyam Pilania.

¹R. M. Martin, *Nature* **400**, 117 (1999).

²J. A. Moriarty and A. K. McMahan, *Phys. Rev. Lett.* **48**, 809 (1982).

³J. C. Boettger and S. B. Trickey, *Phys. Rev. B* **53**, 3007 (1996).

⁴P. K. Lam and M. L. Cohen, *Phys. Rev. B* **27**, 5986 (1983).

⁵M. J. Tambe, N. Bonini, and N. Marzari, *Phys. Rev. B* **77**, 172102 (2008).

⁶I. A. Ovid'ko, *Science* **295**, 2386 (2002).

⁷Y. B. Wang, B. Q. Li, M. L. Sui, and S. X. Mao, *Appl. Phys. Lett.* **92**, 011903 (2008).

⁸I. A. Ovid'ko and A. G. Sheinerman, *Appl. Phys. Lett.* **98**, 181909 (2011).

⁹G. Kresse and J. Furthmüller, *Phys. Rev. B* **54**, 11169 (1996).

¹⁰J. P. Perdew, K. Burke, and M. Ernzerhof, *Phys. Rev. Lett.* **77**, 3865 (1996).

¹¹P. E. Blöchl, *Phys. Rev. B* **50**, 17953 (1994).

¹²M. Jahnátek, J. Hafner, and M. Krajčí, *Phys. Rev. B* **79**, 224103 (2009).

¹³S. K. Yadav, R. Ramprasad, A. Misra, and X.-Y. Liu, *J. Appl. Phys.* **111**, 083505 (2012).

¹⁴L. Li, J.-L. Shao, S.-Q. Duan, and J.-Q. Liang, *Chin. Phys. B* **20**, 046402 (2011).